HHS Public Access

Author manuscript

Arch Biochem Biophys. Author manuscript; available in PMC 2020 March 15.

Published in final edited form as:

Arch Biochem Biophys. 2019 March 15; 663: 239–248. doi:10.1016/j.abb.2019.01.018.

Skeletal muscle mitoflashes, pH, and the role of uncoupling protein-3

S. McBride[a,*], **L. Wei-LaPierre**[b,*], **F. McMurray**[a], **M. MacFarlane**[a], **X Qiu**[c], **D.A. Patten**[a], **R.T. Dirksen**[b], and **M-E. Harper**[a,§]

[a]Department of Biochemistry, Microbiology and Immunology, Faculty of Medicine, University of Ottawa, 451 Smyth Rd., Ottawa, ON, Canada, K1H 8M5

[b]Department of Pharmacology and Physiology, University of Rochester School of Medicine and Dentistry, 601 Elmwood Avenue, Rochester, NY, USA, 14642-8711

[c]Department of Biostatistics, University of Rochester School of Medicine and Dentistry, 601 Elmwood Avenue, Rochester, NY, USA, 14642-8711

Abstract

Mitochondrial reactive oxygen species (ROS) are important cellular signaling molecules, but can cause oxidative damage if not kept within tolerable limits. An important proximal form of ROS in mitochondria is superoxide. Its production is thought to occur in regulated stochastic bursts, but current methods using mitochondrial targeted cpYFP to assess superoxide flashes are confounded by changes in pH. Accordingly, these flashes are generally referred to as 'mitoflashes'. Here we provide regulatory insights into mitoflashes and pH fluctuations in skeletal muscle, and the role of uncoupling protein-3 (UCP3). Using quantitative confocal microscopy of mitoflashes in intact muscle fibers, we show that the mitoflash magnitude significantly correlates with the degree of mitochondrial inner membrane depolarization and ablation of UCP3 did not affect this correlation. We assessed the effects of the absence of UCP3 on mitoflash activity in intact skeletal muscle fibers, and found no effects on mitoflash frequency, amplitude or duration, with a slight reduction in the average size of mitoflashes. We further investigated the regulation of pH flashes (pHlashes, presumably a component of mitoflash) by UCP3 using mitochondrial targeted SypHer (mt-SypHer) in skeletal muscle fibers. The frequency of pHlashes was significantly reduced in the absence of UCP3, without changes in other flash properties. ROS scavenger, tiron, did not alter pHlash frequency in either WT or UCP3KO mice. High resolution respirometry revealed that in the absence of UCP3 there is impaired proton leak and Complex I-driven respiration and maximal coupled respiration. Total cellular production of hydrogen peroxide (H_2O_2) as detected by Amplex-UltraRed was unaffected. Altogether, we demonstrate a correlation between mitochondrial membrane potential and mitoflash magnitude in skeletal muscle fibers that is

*Co-first authors

§ Corresponding author: Professor M-E Harper PhD, Department of Biochemistry, Microbiology and Immunology, Faculty of Medicine, University of Ottawa, 451 Smyth Rd, Ottawa, ON, Canada K1H 8M5; mharper@uottawa.ca.

independent of UCP3 and a role for UCP3 in the control of pHlash frequency and of proton leak- and Complex I coupled- respiration in skeletal muscle fibers. The differential regulation of mitoflashes and pHlashes by UCP3 and tiron also indicate that the two events, though may be related, are not identical events.

Keywords

mitochondrial flashes; superoxide; pH; reactive oxygen species; electron transport chain; uncoupling protein 3; proton leak

INTRODUCTION

Mitochondria are a major cellular source of reactive oxygen species (ROS)[1]. The production of ROS by mitochondria is inherently dependent on redox poise (i.e., the balance between the supply and demand for reducing equivalents) and polarization across the mitochondrial inner membrane (MIM) [1, 2]. An important site of ROS production in mitochondria is the electron transport chain (ETC). There are many forms or types of ROS, including superoxide ($O_2^{\cdot -}$), hydrogen peroxide (H_2O_2) and hydroxyl radical ($^{\bullet}OH$). $O_2^{\cdot -}$is formed at the level of the ETC, which has the reduction of O_2 to water as its final step. Indeed, O_2 is a powerful oxidizing agent and its reduction via the ETC occurs in a sequential fashion, and the associated energy is captured as proton motive force across the mitochondrial inner membrane (MIM). $O_2^{\cdot -}$ is the result of the transient formation of a singlet electron intermediate, and is the primal form of ROS produced by the ETC. When the supply of electrons to the ETC respiratory complexes exceeds the activity of the ETC, there is a slight hyperpolarization of the MIM potential and electrons escape from the complexes to cause the univalent reduction of O_2 to O_2^- [1, 2].

Although toxic at high concentrations, ROS serve as important signaling molecules when maintained within tolerable limits [1, 3, 4]. Controlled ROS emission from mitochondria regulates a variety of important processes, such as increases in phosphorylation cascades through the inhibition of phosphatases as occurs during hypoxic signaling, insulin release, insulin signaling, and adipocyte differentiation [5-7]. To keep ROS levels in balance, mitochondria are equipped with an extensive series of anti-oxidative enzymes and low molecular weight molecules capable of reducing ROS. Of relevance to this work, the production of ROS by mitochondria is thought to be self-regulating through the activation and deactivation of uncoupling proteins −2 and −3 (UCP2 and UCP3), which can act in a negative feedback loop to limit subsequent mitochondrial ROS emission [8,9].

Accurate measurement of cellular ROS levels is highly challenging [10]. Traditionally, ROS detection methods have been reliant on redox-active and ROS sensitive chemicals such as DHE and DCFH-DA, which react to produce fluorescent signals [10, 11]. However, these probes display unfavorable properties, including irreversible oxidation by ROS, particularly when measuring ROS in cellular environments. Thus, while cumulative ROS levels can be determined using these sensors, the sensors are unable to detect dynamic fluctuations in ROS within cells. Focus has shifted to the use of redox- and ROS-sensitive fluorescent proteins that cycle between reduced and oxidized states within the cellular environment.

Thus, the use of such biosensors allows dynamic assessment of changes in cells and organelles. For example, the mitochondrial targeted circularly permuted YFP (mt-cpYFP), allows real-time read-outs of dynamic changes in mitochondrial $O_2^{\cdot -}$ production coupled to a modest transient pH alkalinization depolarization of the MIM, termed mitochondrial flashes or “mitoflashes” [12-14].

Initial studies showed that mitoflashes are coincident with MIM depolarization, reliant on normal functionality of ATP synthase, adenine nucleotide transporter (ANT), and the ETC, and that mitoflash activity is tightly linked to metabolism [12, 13, 15, 16]. Activation of the mitochondrial permeability transition pore (MPTP) is thought to be involved in the generation of mitoflashes, although the exact mechanism for mitoflash genesis and termination remains unclear [12, 15, 17]. Experimental evidence discounts a critical role for the inner membrane anion channel (IMAC) in controlling mitoflash activity [15]. Mitoflashes represent a mixed signal consisting of both a transient burst in superoxide production (70%) coupled to a modest alkalization of the matrix (30%) [14]. The latter is also detected as pH spikes, or “pHlashes” using the genetically engineered pH-specific probe mt-SypHer [18, 19]. Multiple studies have confirmed simultaneous changes in ROS production coincident with pH alkalinization and MIM depolarization across a wide variety of cell types using different probes [14, 18, 20], consistent with a transient burst of mitochondrial ROS production coincident with matrix alkalization being metabolically linked events. Mitoflash activity is increased by superoxide generating agents including menadione, aldrithiol and paraquat and inhibited by antioxidants including tiron, TMPyP, SS-31, and superoxide dismutase-2. Moreover, mitoflash activity is strongly dependent on the proton motive force across the MIM [14] and Complex I activity [21].

Even prior to the identification of UCP2 and UCP3, it was well recognized that slight depolarization of the MIM resulted in decreased emission of ROS from mitochondria [22]. Following the identification of UCP2 and UCP3, a series of studies employing exogenous ROS, or ROS byproducts, concluded that the function of UCP2 and UCP3 is the mitigation of ROS production through a ROS-induced negative feedback loop (reviewed in [23, 24]). Mechanistic details however remain largely unknown. While UCP2 is fairly widely expressed, the expression of UCP3 is limited to a few tissues, including skeletal muscle, brown adipose tissue and cardiac muscle. These are all tissues that rely heavily on fatty acid oxidation, which is associated with high rates of mitochondrial ROS production [25-28]. Genetic knockout of UCP3 in skeletal muscle is associated with oxidative damage [29], while increased UCP3 expression is linked to enhanced fatty acid uptake, transport and metabolism, as well as mitigated ROS damage in muscle [29-35]. Inhibiting UCP2 activity in adult cardiac myocytes by genipin and UCP2 knockdown in neonatal cardiac myocytes slightly increased mitoflash frequency [36]. However, a role for UCP3 in the control of mitoflashes has never been studied. Indeed, the transmembrane protein(s) responsible for governing the depolarization events, regulatory mechanisms, and mechanistic details are unknown. Here we aimed to explore mitoflash and pHlash events in intact muscle cells in the presence or absence of UCP3.

MATERIALS AND METHODS

Mice

Ucp3$^{-/-}$ (UCP3KO) and wild-type (WT) mice on a C57BL/6J background were housed at the University of Ottawa and the University of Rochester School of Medicine and Dentistry. All procedures involving the use of animals were performed according to the principles and guidelines of the Canadian Council of Animal Care and the Animal Care Committee of the University of Ottawa approved the study. The University of Rochester Committee on Animal Resources approved all animal protocols used at their facility. Mice were housed in a facility with controlled temperature, humidity, and light-dark cycle (06:00–18:00) and given free access to rodent chow. Both male and female mice were included for each set of experiments, with equal or roughly equal numbers of both sexes according to availability.

In vivo electroporation of mt-cpYFP cDNA into hindlimb footpads of anesthetized mice

For mitochondrial $O_2^{\cdot -}$ and pH flash determinations, mt-cpYFP and mt-SypHer were transiently expressed in six-month-old WT and UCP3KO *flexor digitorum brevis* (FDB) muscle using an *in vivo* electroporation described previously [13]. Briefly, mice were anesthetized by intraperitoneal injection with 100 mg/kg ketamine, 10 mg/kg xylazine and 3 mg/kg acepromazine. Introduction of 30 μg of DNA (15 μl of 2 μg/μl in 71 mM NaCl) was preceded by 1 h digestion of extracellular matrix material in the footpad with 16 μg of bovine hyaluronidase. In order to deliver electrical pulses for muscle electroporation (100 V/cm, 20 ms duration at a rate of 1 Hz), two 30-gauge needles were placed subcutaneously close to the proximal and distal tendons.

Western blotting

FDB muscles were lysed in RIPA buffer supplemented with protease inhibitor cocktail (Sigma P8340) using a MagNA Lyser (Roche). Protein was quantified using a BCA assay. 50 ug of muscle homogenate protein were loaded into each lane of a Bio-Rad minigel system. Following SDS-PAGE, blots were incubated with primary antibodies for UCP3 (AbCam 3477 at 1:1000) and for tubulin (Sigma T6199 at 1:5000), and with their corresponding conjugated secondary antibodies (Promega W4011, and W4021 at 1:2,000) for autoradiographic imaging.

FDB muscle fiber isolation

One week post electroporation, single FDB muscle myofibers were isolated using an enzymatic digestion protocol described previously [13]. FDB muscles of 6-month-old mice were removed and digested in 1.2 mg/mL collagenase A in regular rodent ringer (RRR) solution for 1 h at 37 °C with agitation. Tissue was dissociated by trituration and plated on glass bottom dishes and allowed to settle for >30 min. Single myofibers were transferred to culture medium (1:1 DMEM/F12, 2 % fetal bovine serum and 1 % penicillin and streptomycin) and kept at 37 °C and 5 % CO_2. For mitoflash measurements, isolated myofibers were transferred to RRR solution containing 10 mM glucose and 20 nM tetramethylrhodamine ethyl ester (TMRE) 10 min prior to imaging in order to permit simultaneous monitoring of both mitoflash events and changes in mitochondrial membrane

potential. For pHlashes measurements, FDB fibers were transferred to TMRE solution with or without 10mM tiron 30 min before measurements.

Confocal microscopy

Mt-cpYFP, mt-SypHer and TMRE fluorescence were monitored by confocal imaging as described previously [13]. Time-lapse images were captured using a SuperFluor 40x (1.3 NA) oil immersion objective over 124 s at a rate of 1.24 s/frame. Images were acquired using a Nikon Eclipse C1 Plus confocal microscope (Nikon Instruments, NY, USA). Mt-cpYFP, mt-SypHer and TMRE fluorescence were excited using 488 nm, 488nm and 543 nm lasers and their emissions were detected at 515/30 nm, 515/30 nm and 605/75 nm, respectively.

Event detection and analysis

Time-lapse images acquired by confocal imaging of mt-cpYFP, mt-SypHer and TMRE were aligned in Image J software (NIH, Bethesda, MD) and mitoflash events were detected using a previously described Matlab-based software, Flash Collector (University of Rochester, Rochester, NY) [13]. Flash frequency, amplitude, duration, and area were calculated directly by the analysis program.

Analyses of spatially and temporally linked mitochondrial depolarization events were conducted using Image J software. Flash Collector identified mitoflash regions of interest were traced onto imported image stacks for the TMRE channel and measurements of fluorescence intensity over time were then calculated. Calculations of event amplitude ($\Delta F/F_o$) were carried out for changes in TMRE fluorescence across all time-lapse images acquired. The data points were plotted using linear regression and the correlation was evaluated using a Pearson correlation test.

Electron microscopy

FDB muscles from 6-month-old mice were removed, fixed (2.5 % glutaraldehyde, 2 % paraformaldehyde in phosphate buffered saline, pH 7.4), and stored at 4 °C until preparation for imaging. Muscle was embedded in LR white (Marivac, Quebec, Canada) and thin sections were cut using a Leica Ultracut E Ultramicrotome. Sections were counterstained with lead citrate and uranyl acetate and digital images of muscle longitudinal fiber slices were taken using a JEOL 1230 transmission electron microscope at 60 kV adapted with a 2×2 K bottom-mount CCD digital camera (Hamamatsu, Japan) and AMT software. Subsequently, mitochondrial areas were traced and quantified using Image J software.

Measurement of mitochondrial O_2 consumption and H_2O_2 emission in permeabilized mouse myofibers

High-resolution respirometry was performed as described previously [37]. In a separatecohort of mice, white and red *gastrocnemius* were removed and immediately placed inice-cold biopsy preservation solution (BIOPS; 2.77 mM CaK_2EGTA, 7.23 mM K_2EGTA, 5.77 mM Na_2ATP, 6.56 mM $MgCl_2{\cdot}6H_2O$, 20 mM taurine, 15 mM Na_2Phosphocreatine, 920 mM Imidazole, 0.5 mM DTT, 50 mM MES; pH 7.1). Fibers were permeabilized by incubation in 2 ml of BIOPS with 50 μg/ml saponin for 30 min at 4 °C. Samples were then

washed with a mitochondrial respiration medium (MIRO5; 0.5 mM EGTA, 3 mM $MgCl_2 \cdot 6H_2O$, 20 mM taurine, 10 mM KH_2PO_4, 20 mM HEPES, 110 mM D-sucrose, 0.1% BSA, 60 mM lactobionic acid; pH 7.1) for 10 min at 4 °C. 1-2 mg of muscle bundles were blotted dry and the wet weight was recorded. Measurements of oxygen consumption were performed in duplicate and obtained at 37 °C in MIRO5 using the Oxygraph-2k (Oroboros, Innsbruck, Austria). Measurements were performed in a hyperoxygenated chamber to prevent any potential oxygen diffusion limitation. The following substrates and compounds were added in sequence: malate (2 mM), octanoyl carnitine (200 μM), ADP + Mg^{2+} (5 mM), pyruvate (5 mM), glutamate (10 mM), succinate (10 mM), ADP + Mg^{2+} (5 mM), cytochrome c (10 μM), oligomycin (5 μM), antimycin A (2.5 μM), ascorbate (2 mM) and TMPD (0.5 mM), and NaN_3 (100 μM). Malate and octanoyl carnitine were added to determine adenylate free leak respiration (L_N). ADP was subsequently added to determine maximal electron flow through electron-transferring flavoprotein (ETF) and fatty acid oxidative capacity (P_{ETF}). Submaximal state 3 respiratory capacity through Complex I (P_{CI}) was determined following the addition of pyruvate and glutamate. Succinate and ADP were then added to determine maximum oxidative phosphorylation capacity (P_{CI+CII}). Cytochrome c was added to test the integrity of the outer mitochondrial membrane. In all preparations, addition of cytochrome c caused <±10% increase in respiration, and therefore, none were excluded. Antimycin A was added to inhibit Complex III and terminate respiration in order to determine non-mitochondrial oxygen consumption in the chamber. All values were corrected for residual oxygen consumption.

Measurements of H_2O_2 production were performed in a single run and obtained at 37 °C in ROS buffer (120mM KCl, 20mM HEPES, 10mM KH_2PO_4, 2.86mM $MgCl_2$, 0.2mM EGTA, 0.02% BSA; pH7) using the Oxygraph-2k (Oroboros, Innsbruck, Austria). The following substrates and compounds were added in sequence: Amplex UltraRed (10 μM), horseradish peroxidase (1.25 U/ml), malate (2 mM), octanoyl carnitine (200 μM), succinate (10 mM), ADP + Mg^{2+} (5 mM), oligomycin (5 μM), FCCP (0.25 μM titrating up to four times). In addition, two injections of 41 nM H_2O_2 were used to calibrate the data.

Statistics

Results are expressed as mean±SEM. Statistical analyses were carried out using two-tailed Student-t tests. A Pearson correlation test was used for correlation analysis between peak mitoflash and TMRE amplitudes. An analysis of variance F test was used to compare the slopes of peak mitoflash and TMRE amplitude relationships between WT and UCP3KO for difference in correlation. $P<0.05$ was considered as statistically significant.

RESULTS

Mitoflash amplitude correlates with the magnitude of spatiotemporally coincident depolarizations of the mitochondrial inner membrane (MIM)

It has been proposed that mitoflashes are controlled by a self-regulating mechanism through which mitochondrial depolarization events are activated by the bursts in $O_2^{\cdot -}$ [17]. If these two events are mechanistically associated, their magnitudes should be correlated. We simultaneously monitored changes in transiently expressed mt-cpYFP and TMRE

fluorescence in FDB fibers from WT and UCP3KO mice using confocal imaging. Quantification of the magnitude of mitoflashes and coincident MIM depolarizations revealed a strong correlation between the two events in fibers from both WT and UCP3KO mice (Figure 1). This correlation is similar in both WT (r^2 = 0.68, slope = −3.0) and UCP3KO muscle fibers (r^2 = 0.72, slope = −3.6; slope analysis between WT and UCP3 KO, ANOVA F test p=0.38). These results indicate that large amplitude mitoflashes are associated with large depolarizations of the MIM, regardless of mouse genotype. Representative western blotting results for UCP3 in FDB muscle of WT and UCP3KO mice are shown in Figure 1C.

Decreased mitoflash area, but no differences in duration, amplitude or frequency in the absence of UCP3

Previous research demonstrates that UCP3 proton leak activity is activated by increases in ROS or ROS byproducts, which serves as a negative feedback loop whereby UCP3 activation decreases ROS production by decreasing the MIM potential [38]. However, the role of UCP3 in the temporal control of endogenous ROS production has never been investigated. In order to assess the contribution of UCP3 in the regulation of mitoflash events in intact cells, we examined FDB fibers isolated from adult WT and UCP3KO mice, in which muscle expression of mt-cpYFP was achieved through electroporation.

Analysis of mitoflashes, using FlashCollector [13], provides a wide array of objective characteristics of these events, including amplitude, time-to-peak, duration, and frequency. Alterations in these parameters provide mechanistic insight into the regulation of these events in a model in which the suspected regulator is not present. Our analyses indicate that mitoflashes in muscle fibers obtained from UCP3KO mice were of similar frequency (10.7±0.5 flashes/1000μm^2/100s for WT vs. 10.8±0.3 for UCP3 KO; n=4, p=0.9, Figure 2A-C), amplitude (0.45±0.0.08 for WT vs. 0.46±0.009 for UCP3 KO; n=4, p=0.6, Figure 2D) or duration (full duration half max FDHM, 2.98±0.0.071s for WT vs. 2.84±0.14s for UCP3 KO; n=4, p=0.40, Figure 2E). Surprisingly, we observed that average mitoflash area is reduced 30% in fibers from UCP3KO mice (0.50±0.03 μm^2 *vs.* 0.72±0.05 μm^2, respectively; n=4, p=0.009, Figure 2F). All observed flash areas were sorted and it was noted that the largest flash area is the same, suggesting that while both genotypes are capable of producing large flashes a difference in the average flash area exists. All other characteristics, including decay constant, time to peak, and full duration were not different between fibers from WT and UCP3KO mice (data not shown).

Mitochondrial size is reduced in muscle from UCP3KO mice

Given our finding of a smaller mitoflash area in single muscle fibers from UCP3KO mice, we next examined mitochondrial size using quantitative morphometry of transmission electron micrographs. Since mitoflash events in muscle occur in single and interconnected mitochondria and do not propagate between mitochondria, we set out to assess whether there are inherent differences in mitochondrial dimensions in FDB muscle from WT and UCP3KO mice. Quantitative electron microscopy analyses revealed a potentially smaller average mitochondrial area in muscle from UCP3KO mice compared to that of WT controls (0.047±0.003 μm^2 *vs.* 0.056±0.002 μm^2; n=4, p=0.06, Figure 3), consistent with the reduced mitoflash area observed in fibers from UCP3KO mice.

Mitochondrial energetics in permeabilized muscle fibers of UCP3 KO are impaired.

Given previous observations that mitoflashes depend on mitochondrial metabolism [15], we examined the effects of loss of UCP3 on mitochondrial energetics in muscle fibers. While the effect of UCP3KO on mitochondrial energetics was previously studied in isolated mitochondria from skeletal muscle [33], the effect of UCP3KO on various states of mitochondrial energetics in intact muscle fibers has not been determined. To do this, we examined energetics in *gastrocnemius*, a muscle group in which UCP3 is highly expressed [39]. In the absence of UCP3, respiration in white *gastrocnemius* was significantly lower in response to the fatty acid octanoyl carnitine (10.59±1.39 pmol/(s*mg) *vs.* 15.94±1.81 pmol/(s*mg) in UCP3KO *vs.* WT, respectively, Figure 4A). We also observed impaired activity of Complex I (44.01±4.75 *vs.* 60.06±3.21 in UCP3KO *vs.* WT, respectively; Figure 4B), and of maximal oxidative phosphorylation (66.45±7.68 pmol/(s*mg) *vs.* 92.68±5.91 pmol/(s*mg) in UCP3KO *vs.* WT, respectively; Figure 4C). Of particular importance, regarding the physiological function of UCP3, is our observation of lower leak respiration in the absence of UCP3 (21.90±2.32 pmol/(s*mg) *vs.* 33.14±2.66 pmol/(s*mg) in UCP3KO *vs.* WT, respectively; Figure 4D). Notably, no differences in mitochondrial content were observed between muscles from WT and UCP3KO mice (Figure 4E). In addition, no significant differences in either Complex I activity (Figure 4G) or maximal oxidative phosphorylation (Figure 4H) were observed between red *gastrocnemius* muscles obtained from WT and UCP3KO mice.

Finally, we used Amplex UltraRed, a fluorimetric detector of H_2O_2, to determine if UCP3 deficiency alters total levels of this form of ROS in white or red *gastrocnemius* muscle under different experimentally imposed metabolic states. No significant differences in H_2O_2 production were observed during either maximal respiration (Figure 4F) or under other metabolic states including adenylate free leak respiration, fatty acid oxidation or state 3 respiration (Complex I) (data not shown).

pHlash activity was reduced in UCP3KO mice.

As mentioned earlier, pHlashes represent a matrix alkalinization component in mitoflashes. Since a reduction in some of the metabolic parameters were observed in UCP3 KO mice, we further examined if pHlash activity is affected using mitochondrial targeted SypHer (mt-SypHer). Seven days following *in vivo* electroporation of the construct, FDB fibers exhibited a robust mt-SypHer signal (Figure 5A-D left panels). Interestingly, pHlash frequency is significantly reduced in UCP3 KO mice (5.99±0.4 flashes/1000μm^2/100s for WT vs. 4.38±0.2 for UCP3 KO; Figure 5A-D right panels & E), with no difference observed in amplitude, duration, and flash area (Figure 5F-H). To examine whether the reduction in pHlash activity is related to mitochondrial ROS production, pHlashes were also measured in the presence of ROS scavenger tiron. The application of tiron did not affect pHlash activity in either WT or UCP3 KO mice (5.8±0.5 5.99±0.4 flashes/1000μm^2/100s for WT with tiron; 4.36±0.5 for UCP3 KO with tiron, Figure 5E), indicating that the reduction of pHlash events is independent of ROS in both genotypes. Correlation analysis between the magnitude of pHflashes and MIM depolarizations revealed a moderate correlation between the two events (Figure 5I; r^2=0.41 for WT and 0.47 for UCP3KO), in contrast to the strong correlation between mitoflash amplitude and magnitude of MIM depolarizations. In line with the

mitoflash correlation results, this correlation is similar in FDB fibers from WT and UCP3KO mice.

DISCUSSION AND CONCLUSIONS

Cellular ROS levels are controlled by many complex processes, but ultimately, ROS levels are dictated from moment to moment by a balance between their rates of production and clearing. ROS production in most cell types occurs to the greatest extent in mitochondria, which are the cellular sites of the majority of reducing and oxidizing (redox) reactions, including the ETC, which in turn uses oxygen as the ultimate electron acceptor. Mitochondrial ROS production is elevated when mitochondrial membrane potential is high, as occurs at, or near, State 4 respiration, when ETC constituents exist primarily in their reduced form. While Complexes I and III have traditionally been accepted as the major sources of ROS production via electron slippage mechanisms, during reduction of FMN/ubiquinone and cytochrome c, respectively, additional sites of mitochondrial ROS production have been identified [2, 40, 41]. Other sites of ROS production with physiological relevance are heavily dependent on both the type of substrate being oxidized and the redox state of the cell; these sites include Complex II (succinate dehydrogenase), alpha-ketoglutarate dehydrogenase, glycerophosphate dehydrogenase, dihydroorotate dehydrogenase, pyruvate dehydrogenase complex and ETF:QO [2, 40-46]. A better understanding of the mechanisms and implications of ROS formation is important because ROS have emerged as key signaling molecules in cell biology [3], and because impaired ROS handling is associated with a wide range of disease states, particularly diseases associated with impaired metabolism, such as diabetes, obesity and cardiovascular diseases [3, 10, 47].

There is a growing recognition that most current methods to assess ROS do not accurately measure them in biologically meaningful ways (*e.g.*, [10]). The high temporal resolution and reversible kinetic characteristic of mitoflashes and pHlashes have the capacity to increase our understanding of ROS and ROS-related mitochondrial events. Mitoflashes are associated with the stochastic generation of quantal bursts of $O_2^{\cdot -}$ by mitochondria across a variety of cell types on a quiescent background [12, 13, 15, 16]. They are also associated with mitochondrial depolarizations and mild matrix alkalization, but the mechanistic details regarding their generation, termination and regulation remain unknown. Confirmation that $O_2^{\cdot -}$ is a major component in these events is based on several key findings: 1) SOD2 knockdown increases mitoflash frequency; 2) SOD mimetics, ROS scavengers and mitochondrial antioxidants decrease their frequency; and 3) anoxia abolishes mitoflash activity [12, 48]. Likewise, the rate of increase in MitoSOX fluorescence increases during each mitoflash, consistent with a burst in $O_2^{\cdot -}$ production during each event [15, 48]. Moreover, mitoflash frequency at a particular age in development was shown to negatively correlate with lifespan in a variety of *C. elegans* models [49].

While the existence of mitoflashes is well–established, it is now clear that we are just beginning to understand the complexities concerning the mechanisms of their generation, regulation and physiological relevance. Each mitoflash is accompanied by the opening of a large channel pore sufficient to result in depolarization of the mitochondrial membrane

potential and loss of large organic molecules [12, 14]. Based on this and the fact that mitoflash activity is inhibited in some, but not all [13, 15], cell types by cyclosporin A and cyclophilin D deficiency, the mPTP is a likely candidate for the large channel pore that opens during a mitoflash event. Although the mPTP is the most probable large pore channel activated during a flash, the exact relationship between mPTP activation and mitoflash activity is yet to be determined. For example, mPTP has been proposed as the trigger of mitoflashes since atractyloside increased flash frequency by promoting the opening of mPTP [12]. Alternatively, superoxide produced during a mitoflash event could activate the mPTP to open, resulting in a depolarization of the MIM potential that inhibits superoxide production by Complex I, and thus, terminates the mitoflash [17].

Given the potential importance of mitoflashes in a variety of ROS mediated events, delineation of the mechanism linking quantum bursts in $O_2{\cdot}^-$ and temporally-linked mitochondrial depolarization would provide important information for future research in mitochondrial ROS signaling/metabolism. In this regard, our results demonstrate a strong positive correlation between mitoflash amplitude and the degree of MIM depolarization (Figure 1). Individual flash analyses revealed that the amplitude of each event was similarly positively correlated in muscle fibers from both WT and UCP3KO mice, consistent with a direct relationship between these two mitoflash components as suggested above. Unfortunately, it was not possible to resolve temporal differences between the two events within the constraints of the temporal resolution of the experiments (1.24 sec/image). The absence of a difference in this relationship between muscle fibers from WT and UCP3KO mice suggests that UCP3 is not a primary determinant of the link between mitoflash activity and depolarization of the MIM potential. It should also be noted that mitochondrial depolarization and mitoflashes are not always temporally linked [17]. Moreover, previous work has established that not every membrane depolarization is accompanied by a mitoflash, although every mitoflash occurs with depolarization [17].

In this study we did not assess the effect of UCP3 knockout on mitochondrial membrane potential. We and others have assessed this before. In the first report on the effects of UCP3KO in mice, we demonstrated in isolated mitochondria from skeletal muscle that mitochondrial membrane potential was ~15mV higher over a range of non-phosphorylating respiration rates in KO vs WT mice [33]. Talbot *et al.* demonstrated a UCP3 dependent effect on mitochondrial membrane potential in their experiments involving ROS activation and GDP inhibition of UCP3 in skeletal muscle mitochondria [50]. Also, Murphy *et al.* demonstrated that superoxide and lipid peroxidation products activate the UCPs, including UCP3, and thereby result in decreases in mitochondrial membrane potential [51]. Moreover, we and others have shown differences in proton leak kinetics (JO2/ membrane potential during non-phosphorylating respiration) as an effect of ‘physiological’ increases in the expression of UCP3 protein (*i.e.*, 2.5-fold) such that respiration at a given membrane potential is increased [52]. Our more recent work has demonstrated that UCP3-dependent proton leak is controlled by glutathionylation, which is dependent on redox potential and reactive oxygen species [53]. Given that UCP3 dependent proton leak is controlled by ROS, redox and post-translationally (glutathionylation) it is therefore not surprising that under some experimental conditions, differences in UCP3-dependent kinetics of proton leak are difficult to detect. This would explain some of the controversy in the field.

We found that mitoflashes area was significantly reduced in fibers from UCP3KO mice compared to that of WT mice (Figure 2F), consistent with the smaller mitochondrial area observed in UCP3KO mice by EM analysis (Figure 3). It is important to note that the respective sizes of the mitoflashes and mitochondrial surface area are very different. In light microscopy, the X-Y optical resolution limit is $d=0.61\lambda/NA$, which in the case of green emission (~550nm) and the objective used in our study (1.4NA) is ~240nm (0.24μm); thus $0.24\times0.24=0.57\mu m^2$, which is approximately what we calculate for UCP3KO. Electron microscopy provides a much higher resolution compared with traditional light microscopy, closer to 0.2nm. This high resolution enables measurement of the actual size of a single mitochondrion. It is likely that, using confocal microscopy, our mitoflash measurements reflect small clusters of mitochondria that "flashed" together. If this is the case, a reduction in mitoflash size in UCP3KO FDB fibers could reflect a disruption of the underlying mitochondria network. The reason for why only mitoflash area (and not pHlash area) was significantly different between WT and UCP3KO is not entirely clear, but may be due to mitoflashes representing a subset of pHflashes. This idea is supported by our results that demonstrate a stronger correlation of TMRE dips with mitoflash amplitudes compared to pHlash amplitudes. While we are the first to observe smaller average mitochondria surface area in muscle of UCP3KO mice, this does not mean that there is a lower total mitochondrial content in the muscle. Indeed, when total mitochondrial content was assessed by cytochrome c oxidase activity (Figure 4E), there were no differences. As with many regulatory mechanisms, redundancy exists such that it is likely that UCP3 is only one of several mitoflash modulators, and the absence of UCP3 may lead to compensation by another mechanism (*e.g.*, ANT activity). Indeed, while the overall phenotype of the UCP3KO mouse is mild, previous investigations have demonstrated increased oxidative stress and decreased FAO in muscle from these mice [29, 54]. Since there are as yet no known specific inhibitors or activators for UCP3, it is difficult to definitively discern the role of UCP3 in governing these events. However, it is well known that even small decreases in MIM potential decrease mitochondrial ROS production and multiple mechanisms exist through which MIM polarization could decrease via possible compensatory mechanisms [53]. Since UCP3 is sensitive to ROS, UCP3-mediated proton leak could regulate certain mitoflash properties (*e.g.*, time course of MIM depolarization and/or pH alkalinization).

Currently, two mechanisms have been proposed for the temporal linkage of mitoflashes and membrane depolarization. Simply put, depolarization may either initiate or assist in terminating the burst in $O_2^{\cdot -}$ production. If UCP3 were in the inactive state, it could contribute to mechanisms initiating ("turn-on") the flash; mechanistically this would involve a metabolically-induced gradual hyperpolarization of the MIM, thereby increasing constitutive ROS production, which then in turn would activate UCP3, causing MIM depolarization. The latter would be observed as a decrease in TMRE signal when used in the non-quench mode as was employed in this study. As a result of the depolarization, the ETC would be stimulated to restore membrane potential through increased ETC function. Increased ETC activity could result in increased electron (e-) slippage causing mitoflashes. Alternatively, if UCP3 were acting in a mechanism to terminate ("turn-off') mitoflashes, increases in ETC function would result in slight hyperpolarization of the MIM, which would lead to increased e- slippage, resulting in a measured burst of $O_2^{\cdot -}$ production. The ROS or

ROS by-products would then activate UCP3-mediated leak mechanisms and thereby induce depolarization of the MIM. However, our results showing the similar relationship between mitoflash amplitude and MIM depolarization in fibers from both WT and UCP3KO mice argues against a critical role for UCP3 in MIM depolarization during each mitoflash event.

The slight reduction in pHlash frequency, but not in mitoflash frequency, observed in UCP3 KO mice clearly indicates that mitoflashes and pHlashes are different events, which argues against the proposed notion that mitoflashes are identical to “pH spikes’ [55-57]. This is further supported by the lack of changes in pHlash activity in the presence of tiron in both WT and UCP3 KO mice. This result is in marked contrast to the fact that tiron reduces mitoflash frequency by half in FDB fibers (13.1±1.5 vs. 6.4±1.0 flashes/1000μm^2/100s in the absence and presence of tiron, respectively, and as previously reported [15]). pHlashes might include the tiron-insensitive/ROS-insensitive component of mitoflashes. However how much the two types of events overlap requires further investigation. Previous work from this group also indicated that mitoflash has a minor pH component [14]. The frequency of mitoflash is slightly higher than pHlash and they have similar amplitude and kinetics. It is possible that pHlashes represent the portion of mitoflashes that have a pH component. Our results showed that UCP3KO only suppressed pHlash activity, but not mitoflash frequency. Since only ~30% of the mito-cpYFP signal during a mitoflash results from pH changes [14], and the reduction of pHlash in UCP3KO is also small (~27%), if pHlashes are indeed the pH component in mitoflashes, this small reduction will be hard to resolve using mitoflashes.

Compared to WT mice, UCP3KO mice exhibit lower respiration rates in white *gastrocnemius*, but similar rates in red *gastrocnemius* (Figure 4). White *gastrocnemius* has higher levels of UCP3 expression, despite reduced mitochondrial content compared to red *gastrocnemius* [58]. While a previous study reported reduced oxygen consumption rates in primary myotubes derived from UCP3KO mice to that of WT controls [54], our results are the first to demonstrate UCP3-dependent differences in mitochondrial energetics as assessed in permeabilized muscle fibers. All previous studies in the literature have examined bioenergetics in isolated mitochondria or in primary cells from skeletal muscle. The *ex vivo* permeabilized muscle fiber system is more physiological because mitochondria retain their reticular structures, which are destroyed in the process of mitochondrial isolations. Moreover, all mitochondria are retained in the preparation, and none are lost, as occurs during mitochondrial isolation procedures. Our findings are consistent with the conclusion that UCP3 is responsible for at least some proton leak in these physiologically relevant muscle preparations.

It was previously shown that there is increased oxidative damage, as measured by lower aconitase activity in muscle of UCP3KO mice [29]. UCP3 has been shown to reduce levels of ROS in primary myotubes cultured for 24 hours in the presence of high glucose [54]. For these determinations H_2O_2 was measured using dichlorofluorescein-diacetate (DCFH-DA) over a 30-minute period. Moreover, muscle-specific over-expression of UCP3 lowers ROS emission from muscle mitochondria [59]. In the latter study ROS was measured as H_2O_2 using the p-hydroxyphenylacetate (PHPA) and horseradish peroxidase in isolated mitochondria over 30-minute incubation periods. Here we observed no significant difference in Amplex-Ultrared detection of H_2O_2 production in white and red *gastrocnemius* muscle

fibers from UCP3KO, compared to WT mice. It is difficult to reconcile these different findings. Given the increased oxidative damage in muscle tissue from mice, it seems clear that UCP3 plays some role, direct or indirect, in protection from oxidative damage. Conflicting observations from *in vitro* studies could be related to differences in the biological preparations (*e.g.*, isolated mitochondria, intact cultured cells, permeabilized myofibers) and/or differences in types or levels of metabolic substrates, and/or differences in the reagents used to detect ROS. Moreover, all known reagents for the detection of ROS, including Amplex-Ultra Red, have limitations (*e.g.*, irreversibility, insensitivity, non-specificity) [10].

Nonetheless, the major findings of the current study include demonstration of a tight correlation between the magnitude of mitochondrial ROS production and the degree of membrane depolarization during mitoflashes in skeletal muscle. These findings strengthen the proposed temporal-spatial link between these parameters and provide support for a role for more than one transmembrane protein regulators in the modulation of skeletal muscle mitoflash activity *in vivo*. Characterization of mitoflash events in UCP3KO and WT mice showed no difference in event duration, frequency, or amplitude. UCP3 deficiency resulted in a statistically significant changes in the area of mitoflash activity. Consistent with these observations, electron microscopy revealed smaller mitochondria in skeletal muscle of UCP3KO mice. In addition, skeletal muscle energetics of white *gastrocnemius* muscle showed reduced proton leak- and Complex I coupled-respiration in skeletal muscle fibers.

ACKNOWLEDGEMENTS:

Authors wish to thank Jian Xuan, University of Ottawa, for her assistance with mouse colonies, and Peter Rippstein, University of Ottawa Heart Institute for assistance with electron microscopy.

FUNDING: This work was funded by the Natural Sciences and Engineering Research Council of Canada (RGPIN 04973 to MEH) and the National Institutes of Health (AR059646 and AR053349). SM was funded by NSERC-CGSM. LW-L was supported by the Academia Dei Lincei Fund. FM was funded by the Destination 2020 University of Ottawa and Ontario Ministry of Research Postdoctoral fellowship.

Abbreviations:

1

(ROS)	reactive oxygen species
(ETC)	electron transport chain
(MIM)	mitochondrial inner membrane
(UCP3)	uncoupling protein-3
(mt-cpYFP)	mitochondrial targeted circularly permuted YFP

REFERENCES:

1. Brand MD, Mitochondrial generation of superoxide and hydrogen peroxide as the source of mitochondrial redox signaling. Free Radic Biol Med, 2016 100: p. 14–31. [PubMed: 27085844]
2. Murphy MP, How mitochondria produce reactive oxygen species. Biochem J, 2009 417(1): p. 1–13. [PubMed: 19061483]

3. Holmstrom KM and Finkel T, Cellular mechanisms and physiological consequences of redox-dependent signalling. Nat Rev Mol Cell Biol, 2014 15(6): p. 411–21. [PubMed: 24854789]
4. Reczek CR and Chandel NS, ROS-dependent signal transduction. Curr Opin Cell Biol, 2015 33: p. 8–13. [PubMed: 25305438]
5. Guzy RD and Schumacker PT, Oxygen sensing by mitochondria at complex III: the paradox of increased reactive oxygen species during hypoxia. Exp Physiol, 2006 91(5): p. 807–19. [PubMed: 16857720]
6. Li N, Li B, Brun T, Deffert-Delbouille C, Mahiout Z, Daali Y, Ma XJ, Krause KH, and Maechler P, NADPH oxidase NOX2 defines a new antagonistic role for reactive oxygen species and cAMP/PKA in the regulation of insulin secretion. Diabetes, 2012 61(11): p. 2842–50. [PubMed: 22933115]
7. Tormos KV, Anso E, Hamanaka RB, Eisenbart J, Joseph J, Kalyanaraman B, and Chandel NS, Mitochondrial complex III ROS regulate adipocyte differentiation. Cell Metab, 2011 14(4): p. 537–44. [PubMed: 21982713]
8. Brand MD and Esteves TC, Physiological functions of the mitochondrial uncoupling proteins UCP2 and UCP3. Cell Metab, 2005 2(2): p. 85–93. [PubMed: 16098826]
9. Mailloux RJ and Harper ME, Uncoupling proteins and the control of mitochondrial reactive oxygen species production. Free Radic Biol Med, 2011 51(6): p. 1106–15. [PubMed: 21762777]
10. McMurray F, Patten DA, and Harper ME, Reactive Oxygen Species and Oxidative Stress in Obesity-Recent Findings and Empirical Approaches. Obesity (Silver Spring), 2016 24(11): p. 2301–2310. [PubMed: 27804267]
11. Dikalov SI and Harrison DG, Methods for detection of mitochondrial and cellular reactive oxygen species. Antioxid Redox Signal, 2014 20(2): p. 372–82. [PubMed: 22978713]
12. Wang W, Fang H, Groom L, Cheng A, Zhang W, Liu J, Wang X, Li K, Han P, Zheng M, Yin J, Wang W, Mattson MP, Kao JP, Lakatta EG, Sheu SS, Ouyang K, Chen J, Dirksen RT, and Cheng H, Superoxide flashes in single mitochondria. Cell, 2008 134(2): p. 279–90. [PubMed: 18662543]
13. Wei L, Salahura G, Boncompagni S, Kasischke KA, Protasi F, Sheu SS, and Dirksen RT, Mitochondrial superoxide flashes: metabolic biomarkers of skeletal muscle activity and disease. FASEB J, 2011 25(9): p. 3068–78. [PubMed: 21646399]
14. Wei-LaPierre L, Gong G, Gerstner BJ, Ducreux S, Yule DI, Pouvreau S, Wang X, Sheu SS, Cheng H, Dirksen RT, and Wang W, Respective contribution of mitochondrial superoxide and pH to mitochondria-targeted circularly permuted yellow fluorescent protein (mt-cpYFP) flash activity. J Biol Chem, 2013 288(15): p. 10567–77. [PubMed: 23457298]
15. Pouvreau S, Superoxide flashes in mouse skeletal muscle are produced by discrete arrays of active mitochondria operating coherently. PLoS One, 2010 5(9).
16. Fang H, Chen M, Ding Y, Shang W, Xu J, Zhang X, Zhang W, Li K, Xiao Y, Gao F, Shang S, Li JC, Tian XL, Wang SQ, Zhou J, Weisleder N, Ma J, Ouyang K, Chen J, Wang X, Zheng M, Wang W, Zhang X, and Cheng H, Imaging superoxide flash and metabolism-coupled mitochondrial permeability transition in living animals. Cell Res, 2011 21(9): p. 1295–304. [PubMed: 21556035]
17. Wei L and Dirksen RT, Perspectives on: SGP symposium on mitochondrial physiology and medicine: mitochondrial superoxide flashes: from discovery to new controversies. J Gen Physiol, 2012 139(6): p. 425–34. [PubMed: 22641637]
18. Azarias G and Chatton JY, Selective ion changes during spontaneous mitochondrial transients in intact astrocytes. PLoS One, 2011 6(12): p. e28505. [PubMed: 22145050]
19. Santo-Domingo J, Giacomello M, Poburko D, Scorrano L, and Demaurex N, OPA1 promotes pH flashes that spread between contiguous mitochondria without matrix protein exchange. EMBO J, 2013 32(13): p. 1927–40. [PubMed: 23714779]
20. Breckwoldt MO, Pfister FM, Bradley PM, Marinkovic P, Williams PR, Brill MS, Plomer B, Schmalz A, St Clair DK, Naumann R, Griesbeck O, Schwarzlander M, Godinho L, Bareyre FM, Dick TP, Kerschensteiner M, and Misgeld T, Multiparametric optical analysis of mitochondrial redox signals during neuronal physiology and pathology in vivo. Nat Med, 2014 20(5): p. 555–60. [PubMed: 24747747]
21. Gong G, Liu X, Zhang H, Sheu SS, and Wang W, Mitochondrial flash as a novel biomarker of mitochondrial respiration in the heart. Am J Physiol Heart Circ Physiol, 2015 309(7): p. H1166–77. [PubMed: 26276820]

22. Starkov AA, The role of mitochondria in reactive oxygen species metabolism and signaling. Ann N Y Acad Sci, 2008 1147: p. 37–52. [PubMed: 19076429]

23. Affourtit C, Crichton PG, Parker N, and Brand MD, Novel uncoupling proteins. Novartis Found Symp, 2007 287: p. 70–80; discussion 80–91. [PubMed: 18074632]

24. Harper ME, Green K, and Brand MD, The efficiency of cellular energy transduction and its implications for obesity. Annu Rev Nutr, 2008 28: p. 13–33. [PubMed: 18407744]

25. Seifert EL, Estey C, Xuan JY, and Harper ME, Electron transport chain-dependent and -independent mechanisms of mitochondrial H2O2 emission during long-chain fatty acid oxidation. J Biol Chem, 2010 285(8): p. 5748–58. [PubMed: 20032466]

26. Woldegiorgis G, Yousufzai SY, and Shrago E, Studies on the interaction of palmitoyl coenzyme A with the adenine nucleotide translocase. J Biol Chem, 1982 257(24): p. 14783–7. [PubMed: 6294078]

27. Benderdour M, Charron G, DeBlois D, Comte B, and Des Rosiers C, Cardiac mitochondrial NADP+-isocitrate dehydrogenase is inactivated through 4-hydroxynonenal adduct formation: an event that precedes hypertrophy development. J Biol Chem, 2003 278(46): p. 45154–9. [PubMed: 12960146]

28. Ciapaite J, Van Eikenhorst G, Bakker SJ, Diamant M, Heine RJ, Wagner MJ, Westerhoff HV, and Krab K, Modular kinetic analysis of the adenine nucleotide translocator-mediated effects of palmitoyl-CoA on the oxidative phosphorylation in isolated rat liver mitochondria. Diabetes, 2005 54(4): p. 944–51. [PubMed: 15793231]

29. Vidal-Puig AJ, Grujic D, Zhang CY, Hagen T, Boss O, Ido Y, Szczepanik A, Wade J, Mootha V, Cortright R, Muoio DM, and Lowell BB, Energy metabolism in uncoupling protein 3 gene knockout mice. J Biol Chem, 2000 275(21): p. 16258–66. [PubMed: 10748196]

30. Aguer C, Fiehn O, Seifert EL, Bezaire V, Meissen JK, Daniels A, Scott K, Renaud JM, Padilla M, Bickel DR, Dysart M, Adams SH, and Harper ME, Muscle uncoupling protein 3 overexpression mimics endurance training and reduces circulating biomarkers of incomplete beta-oxidation. FASEB J, 2013 27(10): p. 4213–25. [PubMed: 23825224]

31. Harmancey R, Vasquez HG, Guthrie PH, and Taegtmeyer H, Decreased long-chain fatty acid oxidation impairs postischemic recovery of the insulin-resistant rat heart. Faseb j, 2013 27(10): p. 3966–78. [PubMed: 23825227]

32. MacLellan JD, Gerrits MF, Gowing A, Smith PJ, Wheeler MB, and Harper ME, Physiological increases in uncoupling protein 3 augment fatty acid oxidation and decrease reactive oxygen species production without uncoupling respiration in muscle cells. Diabetes, 2005 54(8): p. 2343–50. [PubMed: 16046300]

33. Gong DW, Monemdjou S, Gavrilova O, Leon LR, Marcus-Samuels B, Chou CJ, Everett C, Kozak LP, Li C, Deng C, Harper ME, and Reitman ML, Lack of obesity and normal response to fasting and thyroid hormone in mice lacking uncoupling protein-3. J Biol Chem, 2000 275(21): p. 16251–7. [PubMed: 10748195]

34. Hoeks J, Hesselink MK, van Bilsen M, Schaart G, van der Vusse GJ, Saris WH, and Schrauwen P, Differential response of UCP3 to medium versus long chain triacylglycerols; manifestation of a functional adaptation. FEBS Lett, 2003 555(3): p. 631–7. [PubMed: 14675786]

35. Bezaire V, Spriet LL, Campbell S, Sabet N, Gerrits M, Bonen A, and Harper ME, Constitutive UCP3 overexpression at physiological levels increases mouse skeletal muscle capacity for fatty acid transport and oxidation. FASEB J, 2005 19(8): p. 977–9. [PubMed: 15814607]

36. Wang X, Zhang X, Wu D, Huang Z, Hou T, Jian C, Yu P, Lu F, Zhang R, Sun T, Li J, Qi W, Wang Y, Gao F, and Cheng H, Mitochondrial flashes regulate ATP homeostasis in the heart. Elife, 2017 6.

37. Beauchamp B, Ghosh S, Dysart MW, Kanaan GN, Chu A, Blais A, Rajamanickam K, Tsai EC, Patti ME, and Harper ME, Low birth weight is associated with adiposity, impaired skeletal muscle energetics and weight loss resistance in mice. Int J Obes (Lond), 2015 39(4): p. 702–11. [PubMed: 25091727]

38. Mailloux R, Seifert E, Bouillaud F, Aguer C, Collins S, and Harper M, Glutathionylation Acts as a Control Switch for Uncoupling Proteins UCP2 and UCP3. Journal of Biological Chemistry, 2011 286(24): p. 21865–21875. [PubMed: 21515686]

39. Jimenez M, Yvon C, Lehr L, Leger B, Keller P, Russell A, Kuhne F, Flandin P, Giacobino JP, and Muzzin P, Expression of uncoupling protein-3 in subsarcolemmal and intermyofibrillar mitochondria of various mouse muscle types and its modulation by fasting. Eur J Biochem, 2002 269(12): p. 2878–84. [PubMed: 12071950]
40. Bazil JN, Pannala VR, Dash RK, and Beard DA, Determining the origins of superoxide and hydrogen peroxide in the mammalian NADH:ubiquinone oxidoreductase. Free Radic Biol Med, 2014 77: p. 121–9. [PubMed: 25236739]
41. Goncalves RL, Quinlan CL, Perevoshchikova IV, Hey-Mogensen M, and Brand MD, Sites of superoxide and hydrogen peroxide production by muscle mitochondria assessed ex vivo under conditions mimicking rest and exercise. J Biol Chem, 2015 290(1): p. 209–27. [PubMed: 25389297]
42. Adam-Vizi V and Tretter L, The role of mitochondrial dehydrogenases in the generation of oxidative stress. Neurochem Int, 2013 62(5): p. 757–63. [PubMed: 23357482]
43. Eaton S, Control of mitochondrial beta-oxidation flux. Prog Lipid Res, 2002 41(3): p. 197–239. [PubMed: 11814524]
44. Lenaz G, The mitochondrial production of reactive oxygen species: mechanisms and implications in human pathology. IUBMB Life, 2001 52(3–5): p. 159–64. [PubMed: 11798028]
45. Quinlan CL, Orr AL, Perevoshchikova IV, Treberg JR, Ackrell BA, and Brand MD, Mitochondrial Complex II Can Generate Reactive Oxygen Species at High Rates in Both the Forward and Reverse Reactions. J Biol Chem, 2012 287(32): p. 27255–64. [PubMed: 22689576]
46. Fisher-Wellman KH, Gilliam LAA, Lin CT, Cathey BL, Lark DS, and Darrell Neufer P, Mitochondrial glutathione depletion reveals a novel role for the pyruvate dehydrogenase complex as a key H2O2-emitting source under conditions of nutrient overload. Free Radic Biol Med, 2013 65: p. 1201–1208. [PubMed: 24056031]
47. Fujimoto S, Mukai E, and Inagaki N, Role of endogenous ROS production in impaired metabolism-secretion coupling of diabetic pancreatic beta cells. Prog Biophys Mol Biol, 2011 107(2): p. 304–10. [PubMed: 21839765]
48. Huang Z, Zhang W, Fang H, Zheng M, Wang X, Xu J, Cheng H, Gong G, Wang W, Dirksen RT, and Sheu SS, Response to 'A critical evaluation of cpYFP as a probe for superoxide'. Free Radic Biol Med, 2011 51(10): p. 1937–40. [PubMed: 21925593]
49. Shen EZ, Song CQ, Lin Y, Zhang WH, Su PF, Liu WY, Zhang P, Xu J, Lin N, Zhan C, Wang X, Shyr Y, Cheng H, and Dong MQ, Mitoflash frequency in early adulthood predicts lifespan in Caenorhabditis elegans. Nature, 2014 508(7494): p. 128–32. [PubMed: 24522532]
50. Talbot DA, Lambert AJ, and Brand MD, Production of endogenous matrix superoxide from mitochondrial complex I leads to activation of uncoupling protein 3. FEBS Lett, 2004 556(1–3): p. 111–5. [PubMed: 14706836]
51. Murphy MP, Echtay KS, Blaikie FH, Asin-Cayuela J, Cocheme HM, Green K, Buckingham JA, Taylor ER, Hurrell F, Hughes G, Miwa S, Cooper CE, Svistunenko DA, Smith RA, and Brand MD, Superoxide activates uncoupling proteins by generating carbon-centered radicals and initiating lipid peroxidation: studies using a mitochondria-targeted spin trap derived from alpha-phenyl-N-tert-butylnitrone. J Biol Chem, 2003 278(49): p. 48534–45. [PubMed: 12972420]
52. Estey C, Seifert EL, Aguer C, Moffat C, and Harper ME, Calorie restriction in mice overexpressing UCP3: evidence that prior mitochondrial uncoupling alters response. Exp Gerontol, 2012 47(5): p. 361–71. [PubMed: 22406134]
53. Mailloux RJ, Seifert EL, Bouillaud F, Aguer C, Collins S, and Harper ME, Glutathionylation acts as a control switch for uncoupling proteins UCP2 and UCP3. J Biol Chem, 2011 286(24): p. 21865–75. [PubMed: 21515686]
54. Mailloux RJ, Dumouchel T, Aguer C, deKemp R, Beanlands R, and Harper ME, Hexokinase II acts through UCP3 to suppress mitochondrial reactive oxygen species production and maintain aerobic respiration. Biochem J, 2011 437(2): p. 301–11. [PubMed: 21554247]
55. Schwarzlander M, Logan DC, Fricker MD, and Sweetlove LJ, The circularly permuted yellow fluorescent protein cpYFP that has been used as a superoxide probe is highly responsive to pH but not superoxide in mitochondria: implications for the existence of superoxide 'flashes'. Biochem J, 2011 437(3): p. 381–7. [PubMed: 21631430]

56. Schwarzlander M, Murphy MP, Duchen MR, Logan DC, Fricker MD, Halestrap AP, Muller FL, Rizzuto R, Dick TP, Meyer AJ, and Sweetlove LJ, Mitochondrial 'flashes': a radical concept repHined. Trends Cell Biol, 2012 22(10): p. 503–8. [PubMed: 22917552]

57. Schwarzlander M, Wagner S, Ermakova YG, Belousov VV, Radi R, Beckman JS, Buettner GR, Demaurex N, Duchen MR, Forman HJ, Fricker MD, Gems D, Halestrap AP, Halliwell B, Jakob U, Johnston IG, Jones NS, Logan DC, Morgan B, Muller FL, Nicholls DG, Remington SJ, Schumacker PT, Winterbourn CC, Sweetlove LJ, Meyer AJ, Dick TP, and Murphy MP, The 'mitoflash' probe cpYFP does not respond to superoxide. Nature, 2014 514(7523): p. E12–4. [PubMed: 25341790]

58. Boss O, Samec S, Paoloni-Giacobino A, Rossier C, Dulloo A, Seydoux J, Muzzin P, and Giacobino JP, Uncoupling protein-3: a new member of the mitochondrial carrier family with tissue-specific expression. FEBS Lett, 1997 408(1): p. 39–42. [PubMed: 9180264]

59. Seifert E, Estey C, Xuan J, and Harper M, Electron Transport Chain-dependent and - independent Mechanisms of Mitochondrial H2O2 Emission during Long-chain Fatty Acid Oxidation. Journal of Biological Chemistry, 2010 285(8): p. 5748–5758. [PubMed: 20032466]

Highlights:

- Mitoflash intensity is positively correlated with the magnitude of membrane depolarization, independent of UCP3
- UCP3 controls pHlash frequency in skeletal muscle fibers
- UCP3 controls proton leak and Complex-I driven respiration in muscle fibers
- Mitoflashes and pHlashes are not identical events

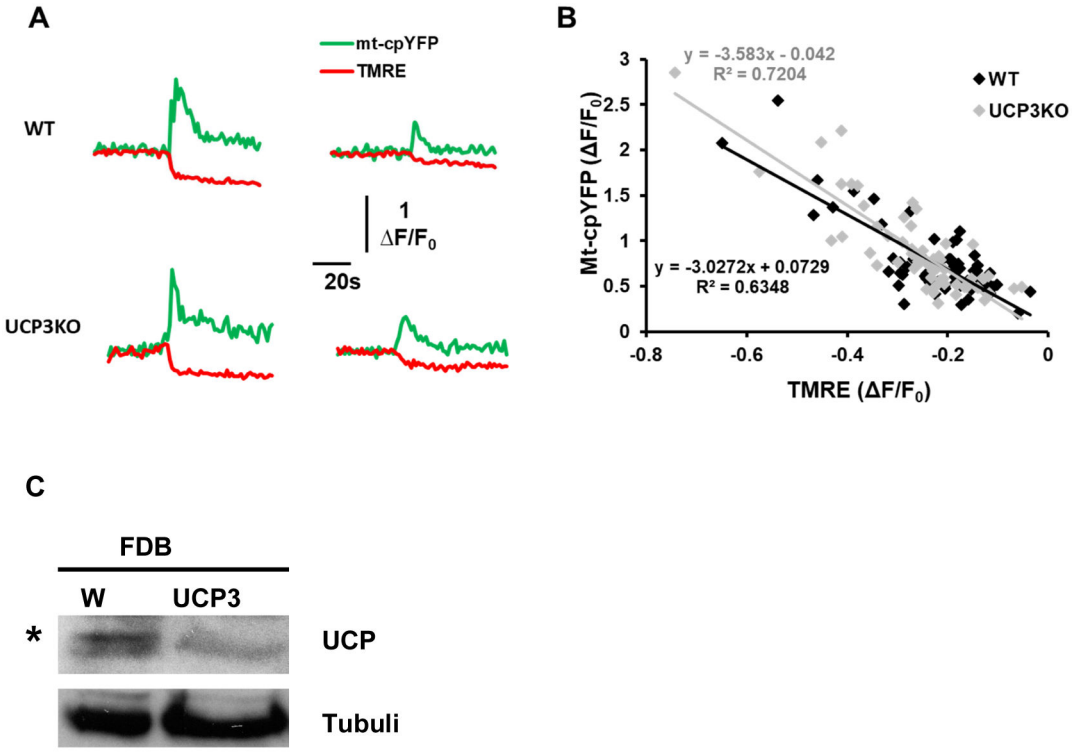

Figure 1. Positive correlation between flash intensity and the magnitude of MIM depolarization in both WT and UCP3 KO mice.

A. Representative traces from WT (top) and UCP3 KO (bottom) FDB fibers showing different amplitude of mitoflashes corresponding to different amplitude of MIM depolorisation (TMRE fluorescence). **B.** Correlation analyses of the amplitude of mt-cpYFP flashes and concomitant mitochondrial depolarization events (TMRE fluorescence). (n=60-112 events for each genotype, $p<0.0001$). **C.** Representative western blot of UCP3 in FDB muscle from WT and UCP3 KO mice. Asterisk indicates the top band at ~34kDa, which is missing in UCP3KO muscle.

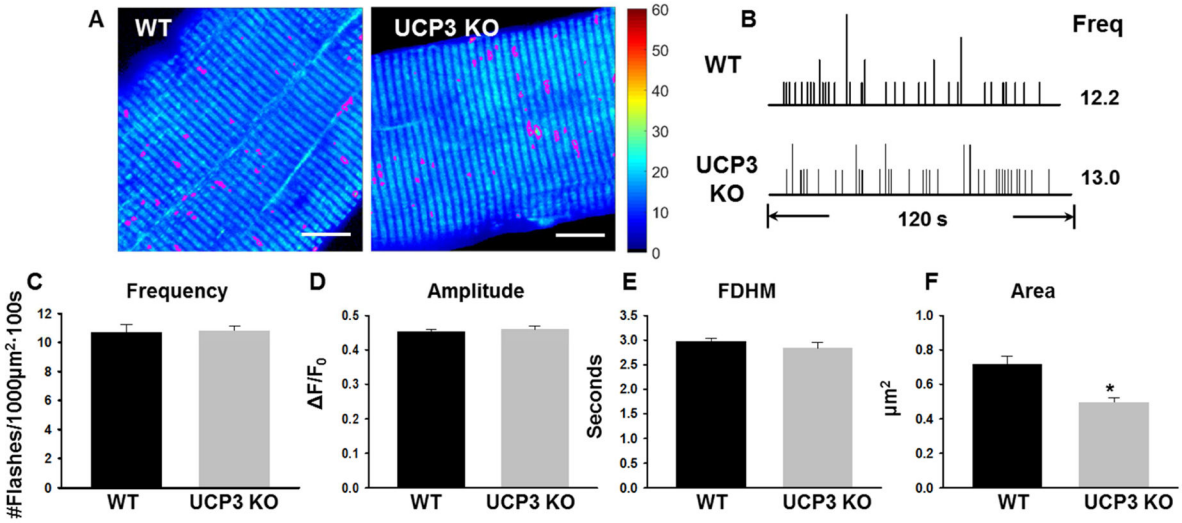

Figure 2. Mitoflash activity in FDB fibers from UCP3KO mice was unaltered, with a slight reduction in the size of flashes.

A. representative standard deviation maps automatically generated by "flash collector" indicating all the events detected (circled in magenta) in the cell. **B.** a tic registry showing the occurrence of every single events during the 120s recording. Calculated frequency for the particular cell is indicated on the right. **C-F.** Average (±SEM) flash frequency (C), amplitude (D), FDHM (E) and flash area (F) for WT and UCP3 KO mice. N=4 mice with each genotype. *significantly different from WT, unpaired, two tail *Student-t* test, $p<0.05$. Scale bars: 10 μm.

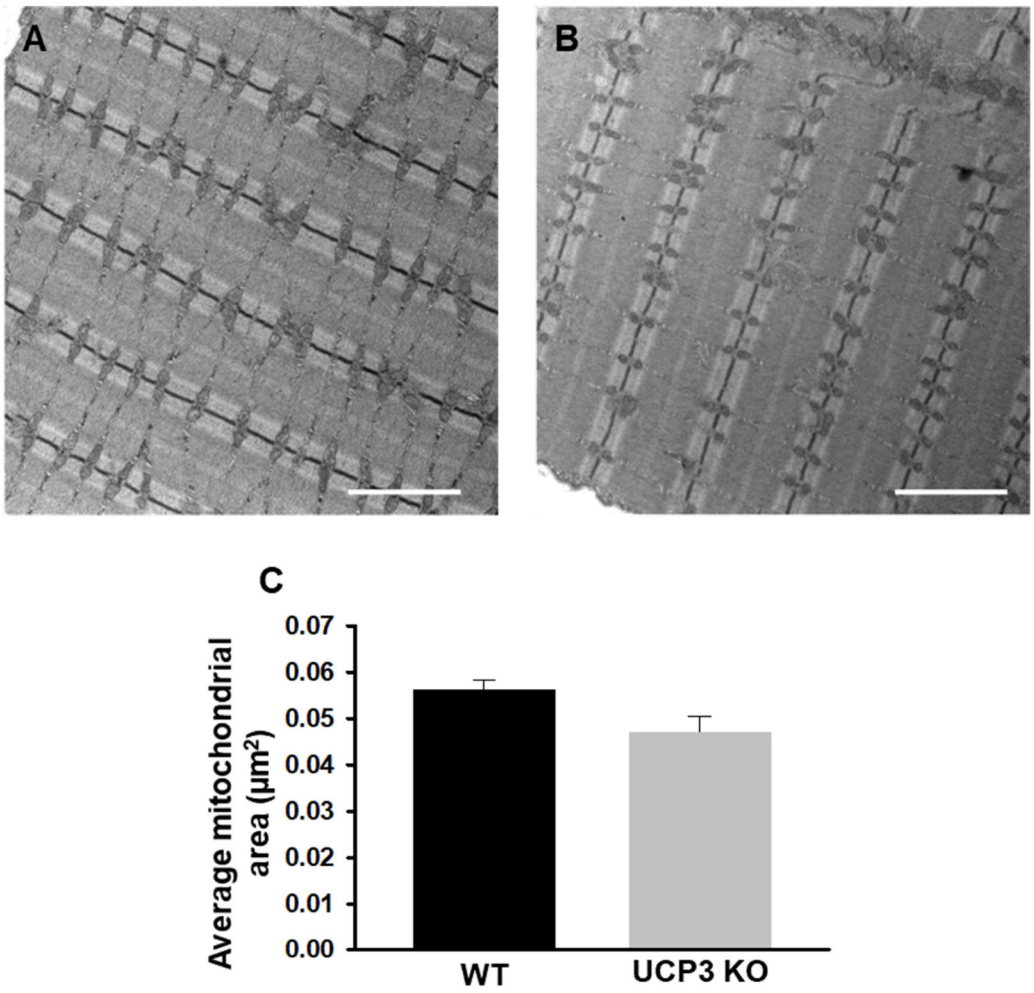

Figure 3. Mitochondrial area in FDB muscle fibers from UCP3KO mice.

A-B) Representative EM images used for analysis of mitochondrial area obtained from FDB muscles of WT **(A)** and UCP3KO **(B)** mice. **C)** Average (±SEM) area of measured mitochondria. Mitochondrial area in UCP3KO muscle was potentially smaller than that in muscle of WT mice. n=4 mice, two-tail *Student-t* test., p=0.06. Scale bars: 2μm.

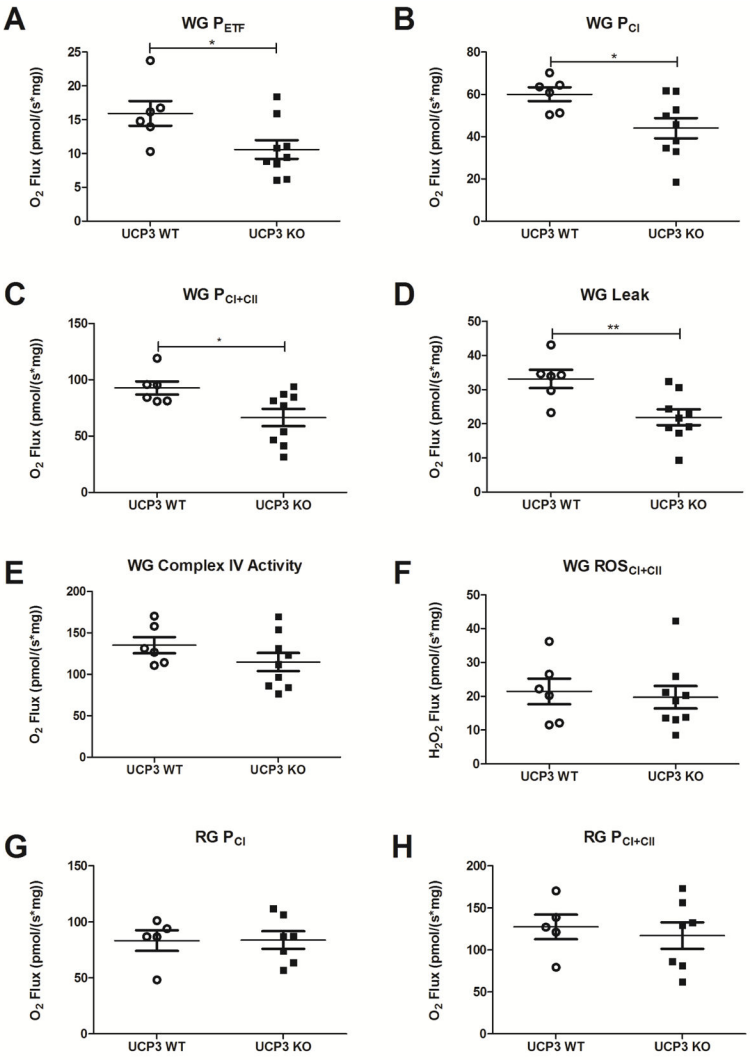

Figure 4. Mitochondrial energetics in permeabilized white and red *gastrocnemius* muscle fibers from WT and UCP3KO mice.

Oxygen flux data for permeabilized white *gastrocnemius* muscle fibers are shown for **A)** fatty acid oxidative capacity (P_{ETF}), **B)** Complex I (P_{CI}), **C)** maximal oxidative phosphorylation capacity (P_{CI+CII}), and **D)** Leak. **E)** Estimation of mitochondrial content using TMPD and ascorbate. **F)** H_2O_2 flux at maximal oxidative phosphorylation capacity in white *gastrocnemius*. Oxygen flux data for permeabilized red *gastrocnemius* muscle fibers are shown for **G)** Complex I (P_{CI}) and **H)** maximal oxidative phosphorylation capacity (P_{CI+CII}). (Average±SEM) (UCP3WT n=5-6, mice; two-tail *Student-t* test.

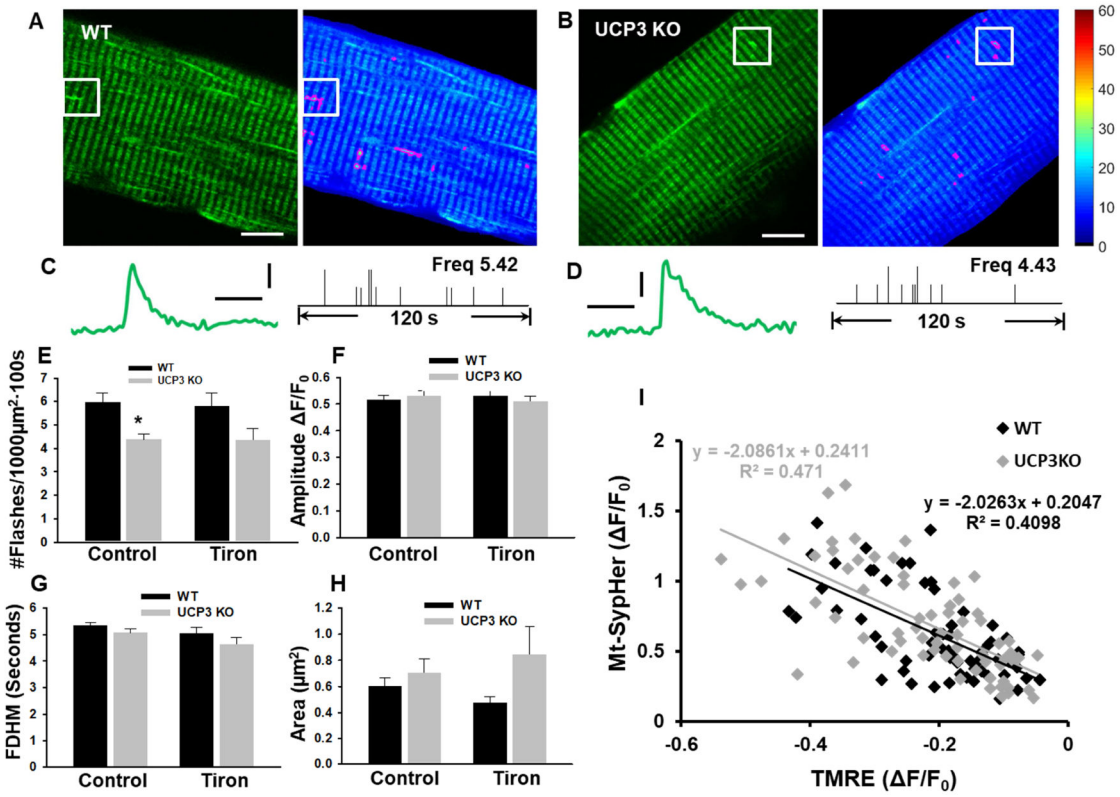

Figure 5. pHlash activity is reduced in FDB fibers from UCP3 KO mice.

A) A representative image for mt-SypHer fluorescence (left) and standard deviation map (right) generated by "flash collector" during event detection in a WT FDB fiber. Active mitochondria are circled in magenta. Boxed area indicates an active flash. **B**) same as **A,** except for from a FDB fibers from a UCP3 KO mouse. **C**) left; plotted trace of mt-SypHer fluorescence for the flash in the boxed area in **A**. right: a tic registry showing the occurrence of each events during the 120s recording. Calculated frequencies were indicated above the registry. **D)** same as C, except for the traces and registry corresponding to the cell in **B. E-H**) Average (±SEM) flash frequency (**E);** amplitude **(F)**; FDHM **(G)**; and flash area **(H)** for WT and UCP3 KO mice. N=5-17 mice for WT and UCP3 mice with and without tiron. (**I**) Correlation analyses of the amplitude of pH flashes (mt-SypHer) and concomitant mitochondrial depolarization events (TMRE fluorescence). (n=64 events for WT; n=68 events for UCP3KO) *significantly different from WT, unpaired, two tail *Student-t* test, $p<0.05$. Scale bars for A: 10 μm; Scale bars for C &D: vertical, 0.2 $\Delta F/F_0$; horizontal, 20s.